Transformation of secondary steelmaking slags towards a hydraulic binder via controlled cooling and post-processing

Y. Pontikes, L. Kriskova, D. Geysen, P. T. Jones, M. Guo, B. Blanpain*
Centre for High Temperature Processes and Sustainable Materials Management,
Department of Metallurgy and Materials Engineering, KU Leuven, Belgium

Abstract: This work explores the possibility of transforming secondary steelmaking slags to a cementitious binder by: a) high cooling-rate solidification and b) mechanical activation via high energy milling in a bead mill. Industrially produced and synthetic slags with various basicities were used in the experiments. Hydraulic activity was evaluated by means of isothermal calorimetry, scanning electron microscopy (SEM), thermogravimetry (TGA) and quantitative X-ray diffraction analysis (QXRD). For the study of the cooling path, a melt spinning granulation device was employed in addition to water quenching experiments. Results demonstrate that the beta to gamma-$2CaO.SiO_2$ transformation can be suppressed and that the end product is hydraulically active upon mixing with water. For the mechanically activated samples, 2h and 6h milling resulted in partial amorphisation and significant increase of hydraulic activity compared to the as-received slags. The work concludes with a proposed hydration behavior for the major slag phases.

Keywords: secondary steelmaking slag, quenching, melt spinning, mechanical activation, cement.

1. Introduction

With an EU-wide clinker benchmark production of 0.78t of CO_2 per ton of grey clinker [1] and an annual worldwide cement production close to 2800Mt [2], the cement industry contributes to approximately 5% of the total anthropogenic CO_2 emissions [3]. Revisions are investigated in the manufacturing process and in the selection of raw materials to reduce the industry's footprint. On the "Cement Technology Roadmap 2009" [4], possible transition paths for the industry are presented in order to reduce by 50% the global CO_2 emissions by 2050. Reducing the clinker content in cement (the "clinker to cement ratio", or "clinker factor") is one of the primary paths. The use of stainless steel slag as a supplementary cementitious material can be of great interest in this context. Indeed, even though stainless steel slag production is an insignificant fraction compared to the annual global cement production, it is of interest for specific regions, Europe, being one.

The potential of secondary steelmaking slag to be used as hydraulic binders has been investigated before. Sheh *et al.* [5] observed particle size growth on ground stainless steel AOD slag when mixed with water and suggested it indicates pozzolanic or hydraulic properties. Wang and Chen stated that a composite cement can be formed when a proper amount of stainless steel AOD slag is added [6]. Faraone *et al.* [7] claim that steelmaking slag is not an inert material whereas Setién *et al.* [8] observed that LM slag developed cementitious properties when it reacted with atmospheric moisture. Rodriguez *et al.* [9] used LM slag in masonry mortars as a partial replacement for sand and cement. Finally, Shi *et al.* [10, 11] studied the cementitious properties of chemically activated LM slag. Even though it is difficult to make general statements regarding the valorisation of steel and stainless steel slag, the cited works do demonstrate a clear potential for these materials.

Despite the work in the field, it is characteristic that in all above-cited works little emphasis is given to the possibility of modifying the slag, either during production or in a post-production operation. Still, work in other slags or materials has provided promising results. For instance, the effect of doping and subsequent rapid cooling has been addressed recently on a steel slag after reduction [12] whereas research on granulated blast furnace slag and fly ash, among other materials, has demonstrated the effectiveness of mechanical activation as a means to increase the hydraulic reactivity [13-15].

In the present study, the effect of cooling and of mechanical activation on the hydraulic properties of high basicity slags was studied, aiming to assess the possibility of using these materials as hydraulic binders.

2. Experimental

Synthetic slags were prepared by mixing analytical grade oxides/carbonates. The various basicities (CaO/SiO_2) were chosen to cover part of the compositional range of LM and AOD slags. The chemical composition of synthetic and industrial samples tested is presented in Table 1.

Table 1. Chemical composition of synthetic slags. n.d.: not determined.

	I	II	III	IV	LM	AOD
CaO	52.4	54.7	56.7	58.5	51.5	55.6
SiO_2	32.7	30.4	28.4	26.6	28.3	31.7
MgO	6.5	6.5	6.5	6.5	11.3	9.8
Al_2O_3	1.3	1.3	1.3	1.3	1.2	1.2
TiO_2	1.1	1.1	1.1	1.1	n.d.	n.d.
Cr_2O_3	0.0	0.0	0.0	0.0	3.9	0.3
CaF_2	6.0	6.0	6.0	6.0	n.d.	n.d.
Others	0.0	0.0	0.0	0.0	3.8	1.4

For the rapid quenching experiments, the synthetic slags were melted in an induction-heating set up using graphite crucibles. The heating cycle was RT to 1700 °C ± 30 °C within 7 min, followed by an isothermal step at this temperature for an additional 7 min in order to enhance dissolution and homogenization. The molten slag was released from the crucible by rising up the graphite pin blocking the orifice in the bottom of the crucible. The melt was either granulated on a rotating copper wheel or quenched in water. All the experiments were performed in protective atmosphere of argon. The rapidly cooled slags were collected and the fraction > 250 μm was used.

For the mechanical activation, a bead mill (Dispermat SL-12-C1, VMA) was used. The milling was carried out with approximately 10 wt.% slag in ethanol suspension at 5000 rpm using 1 mm zirconia balls. To determine the effect of milling time on the powder fineness, the LM slag was milled for 2 h and 6 h. Based on the results obtained in terms of hydraulic reactivity, the AOD slag was only milled for 6 h.

The particle size distribution of the slags was determined by laser scattering (MasterSizer Micro Plus, Malvern). The surface area was determined by nitrogen sorption method BET (Micromeritics TriStar 3000 V6.04 A). Prior to BET analysis, the samples were dried at 150 °C for 12 h. The mineralogy of the materials was determined by X-ray powder

diffraction analysis (XRPD, D500 Siemens). Diffraction patterns were measured in 2θ range of 10-70° using CuKα radiation of 40 kV and 40 mA, with a 0.02° step size and step time of 4s. Quantitative analysis was performed by "Topas® Academic" software.

The hydraulic reactions were monitored by isothermal conduction calorimetry (TAM Air device, TA Instruments) at 20 °C. Analysis was performed on pastes with water to solid ratio (w/s) equal to 0.75 for the rapidly quenched slag and 1.0 for the mechanically activated slags. For the study of the hydration products, the paste samples were stored in sealed plastic capsules for 3, 7 and 28 days. After the designated period of time, the samples were crushed to powder and the hydration was stopped by vacuum-drying (Alpha 1-2 LD, Martin Christ) as suggested elsewhere [16]. Powder samples were subjected to thermal analysis using simultaneous TGA/DSC (STA 409 PC Luxx®, Netzsch). The samples were heated at either 5 °C/min or 10 °C/min in a continuous N_2 flow up to 1000 °C. Microstructural characterization was performed on scanning electron microscope (SEM XL30, Philips). The granulated samples were etched for 5 s in 3% nital. To avoid structural destruction of the hydrated phases during drying, pastes samples were kept at 50 °C for 2 days.

3. Results and discussion for melt spinning granulation

3.1. Slag characterisation

Slags granulated on the rotating copper wheel resulted to spherical and ribbon like particles, Fig. 1(a). The max diameter of stabilised granules was <1 cm, however, the granules were hollow. The thickness of the walls is comparable to the maximum thickness of stabilised ribbon-like slags, i.e. 0.3 mm approximately. Part of the granules disintegrated in the following days. This phenomenon, known as late falling [17] was more pronounced on the lower-basicity slags.

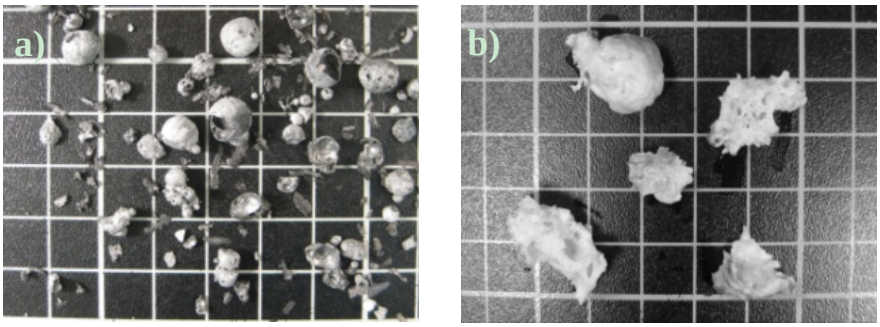

Figure 1. Stabilised slag after (a) granulation, (b) water quenching, mesh dimension is1cm.

Water quenching resulted into volumetrically stable, brittle and porous materials, typically between 2-3cm, Fig. 1(b). The shell of the granules was very thin, typically less than 1mm. The slag with basicity 2.2 was not studied.

3.2. Mineralogy and microstructure

The basicity of the slags has a strong effect on the mineralogical composition, Table 2. In all cases bredigite, merwinite and dicalcium silicate (C_2S) polymorphs are the major phases. At higher basicity the amount of C_2S increases at the expense of merwinite and bredigite and MgO is present as in the form of periclase. Water quenched slags are qualitatively comparable in terms of mineralogy with the ones from melt spinning granulation. However, the

ratio β-C_2S/γ-C_2S is higher in the former case compared to the granulated samples. Still, the evolution of mineralogy as the basicity increases presents a similar trend in both solidification techniques. This indicates that despite the difference between moderately high and high cooling rates on the mineralogy, the main influence arises from the chemical composition.

SE micrographs of granulated slag are shown in Fig. 2(a)-(d). At low basicities, β-C_2S solidified into egg-shape nodules with lamellar structure, resembling belite grains occurring in cement clinker. The typical lamellar structure of β-C_2S comes from the twinning along {100} and/or {001} lattice planes. This twinning arises when a higher temperature form of C_2S transforms into β form on cooling [18]. The system is composed also of merwinite and bredigite, which represent the matrix in the form of angular, randomly distributed grains, Fig. 2(a). As the basicity increases, β-C_2S becomes the main phase constituting now most of the matrix. The other Mg containing phases are located at the grain boundaries, mostly in the form of dendrites, Fig. 2(d). The average grain size of C_2S decreases as the basicity increases, being less than 10 μm for higher basicities (III, IV).

Table 2. Mineralogical composition of granulated and water quenched (WQ) slags. b.d.l. is below detection limit.

	I		II		III		IV
	granulated	**WQ**	**granulated**	**WQ**	**granulated**	**WQ**	**granulated**
β-C_2S	7.3	18.8	20.6	28.7	67.8	81.9	49.7
γ-C_2S	b.d.l.	b.d.l.	19.7	9.9	18.8	4.2	15.7
Merwinite	41.5	43.3	9.3	5.2	b.d.l.	b.d.l.	1.2
Bredigite	44.4	35.3	41.3	49.3	0.8	3.8	4.4
Fluorite	2.3	1.8	4.6	3.7	5.0	2.8	2.9
Cuspidine	4.6	0.9	b.d.l.	b.d.l.	b.d.l.	b.d.l.	b.d.l.
MgO	b.d.l.	b.d.l.	4.8	3.3	7.6	7.3	7.4
Akermanite	b.d.l.	b.d.l.	b.d.l.	b.d.l.	b.d.l.	b.d.l.	2.5
C_3S	b.d.l.	b.d.l.	b.d.l.	b.d.l.	b.d.l.	b.d.l.	16.2

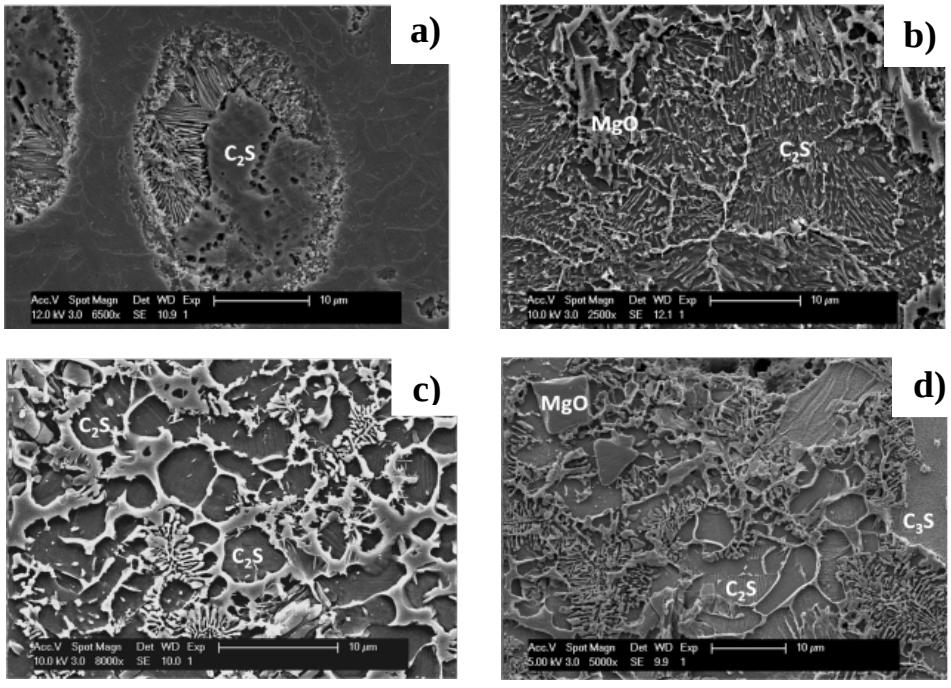

Figure 2. SE micrographs of slag stabilised by granulation (a) I, (b) II, (c) III, (d) IV.

3.3. Hydraulic behaviour

As the mineralogical composition of both granulated and water quenched slags is comparable, only granulated material was used for the study of hydraulic properties. All finely milled slags (with d_{50} around 10μm), besides sample I, showed reactivity when mixed with water, as it is demonstrated by the exothermic peak in the calorimetric measurement, Fig. 3 (a). The curves of cumulative heat release illustrate that the higher the basicity of the material, the higher the heat release (although considerations in terms of absolute values should be performed on the basis of equal fineness of the powder). This is in good agreement with the XRD results where the amount of β-C_2S increases with an increase of basicity. As expected, when the basicity exceeds 2, like in the case of sample IV, C_3S is also formed. This is reflected in the respective calorimetry curve, where a new peak was recorded at 8 h approximately after the hydration started. Other phases present, as merwinite, bredigite, etc are considered to have rather low hydraulic activity [12, 19].

Fig. 3(b) presents the derivatives of TGA (thermogravimetric analysis) curves of all four hydrated slags after 3 days of hydration. The part below 200 °C can be associated with a weight loss due to an interlayer water loss of calcium-silicate hydrates (C-S-H) [20]. The area between 350 °C and 420 °C is associated with the weight loss resulting from the dehydration of brucite [20]. Reactions in the temperature range between 425 °C to 550 °C are primarily associated with the dehydration of $Ca(OH)_2$ [21] and above 550 °C, partially due to CO_2 release arising from the dissociation of carbonates. As the hydration progresses (data not presented), the area of the peaks is growing. In particular, the first peak below 200 °C is more pronounced on the slags with higher basicity. This is a strong indication that the C-S-H content also increases, thus that the hydraulic reactions are on-going and that the amount of β-C_2S is decisive.

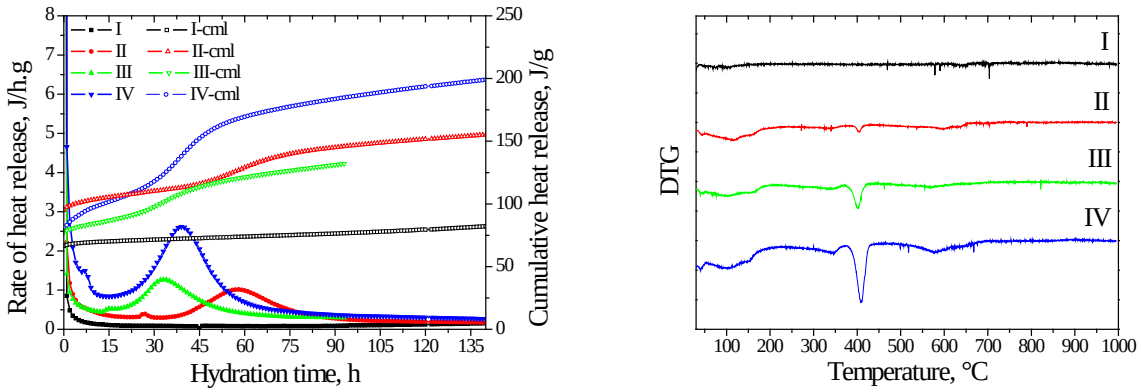

Figure 3. (a) Calorimetry measurements of granulated slags, cml= cumulative; (b) DTG curves of hydrated slags after 3 days.

Results from SEM analysis reveal that the C-S-H phase, Fig. 4 for sample III, exists in flake-like morphology at an early stage and forms a rather compact reticulated network after 28 days of hydration. It is evident that the structure is rather compact already after 3 days of hydration which indicates relatively fast hydration progress. This is in line with the DTG curves, as a clear broad peak is present after 3 days of hydration.

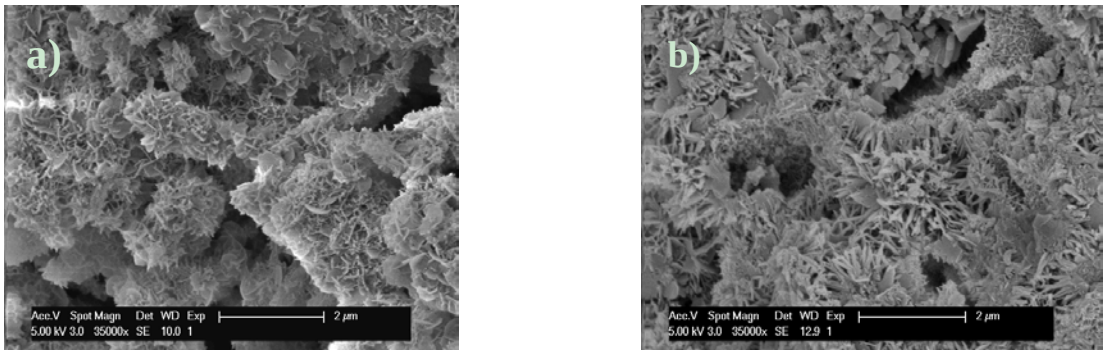

Figure 4. SE micrographs of slag III after (a) 3 days, (b) 28 days of hydration.

4. Results and discussion for mechanical activation

4.1. Slag characterisation

Due to the relatively high magnesium content in the slags, the major phases besides γ-C_2S are merwinite, bredigite and periclase. These phases are generally considered as non-hydraulic or hydrating very slowly [22-24]. Among all the phases present, only β-C_2S is considered to be hydraulic but in both samples its content is negligible, Table 3.

Table 3. Mineral composition of LM and AOD slag as received, in wt.%.

No.	Phase	Theoretical formula	LM	AOD
1	γ – dicalcium silicate	γ – $(CaO)_2.SiO_2$	34	16
2	β – dicalcium silicate	β – $(CaO)_2.SiO_2$	< 1	n/a
3	Merwinite	$Ca_3Mg(SiO_4)_2$	6	37
4	Bredigite	$Ca_{1.7}Mg_{0.3}SiO_4$	7	15
5	Wollastonite	$CaSiO_3$	2	3
6	Periclase	MgO	15	7
7	Cuspidine	$Ca_4Si_2F_2O_7$	10	< 1
8	Fluorite	CaF_2	2	4
9	Magnesiochromite	$MgCr_2O_4$	3	n/a
10	Others/Amorphous		20.0	18

In terms of particle size distribution, the D_{50} of as-received slags equals approximately 19 µm and 55 µm for LM and AOD slag, respectively. After 6 h milling the D_{50} value decreased to 2 µm and 3 µm for LM and AOD slag, respectively. The BET specific surface area of the 6 h milled slag has increased significantly: from a starting value less than 1 m^2/g, the specific surface area became approximately 10 m^2/g for LM and 8 m^2/g for AOD slag after milling. The as-received slag powder consists mostly of irregularly-shaped particles; C_2S grains in particular are characteristic in view of their extensive network of cracks. After 6 h of milling, the particles were smaller and angular.

The results by Rietveld analysis are reported in Table 4 for LM slag (data for AOD not shown). The amount of γ–C_2S, merwinite, bredigite, periclase, fluorite and wollastonite decrease whereas the amount of amorphous phase increases upon milling. Quantification of each mineral in the slag, before and after 6h milling, reveals that γ-C_2S shows relatively

higher degree of amorphisation, 30 % in LM and 58 % in AOD slag, compared to merwinite and bredigite. This is probably linked with the β→γ polymorphic transformations during cooling and the substantial stress generation and crack formation. Only wollastonite was found to be more susceptible to amorphisation due to milling, with 77 % and 64 % change in LM and AOD slag respectively.

4.2. Hydration behaviour

As demonstrated in Figure 5(a), the slags in the as-received state showed only negligible or no heat release at the early stage. However, in both milled samples, a sharp exothermic peak occurred after 17 h and 25 h for LM and AOD slag respectively. These peaks are primarily associated with heat released due to hydration reactions; other dissolution reactions may be also contributing to a small extent. The cumulative energy released within the first 80 h (highest reaction rate) equals to 61 J/g for LM and 52 J/g for AOD milled slags. For comparison purposes, the heat released by OPC with BET surface lower than 1 m^2/g is around 200 J/g. For 2 h milling, the total heat released is approximately 30 J/g, an indication that prolonged milling has a significant effect on the hydraulic reactivity.

The increased reactivity is a consequence of both increased specific surface area and of enhanced stored energy, resulting from the structural defects introduced during milling. This combined activation effect can be clearly seen by closer examination of the part of the graphs where the exothermic peaks are present, e.g. between 10 h and 80 h of hydration. It is calculated that the ratio of total heat release during the mentioned time period over the surface area of reacting powders increases as milling increases, an indication that the surface is not the only factor influencing reactivity.

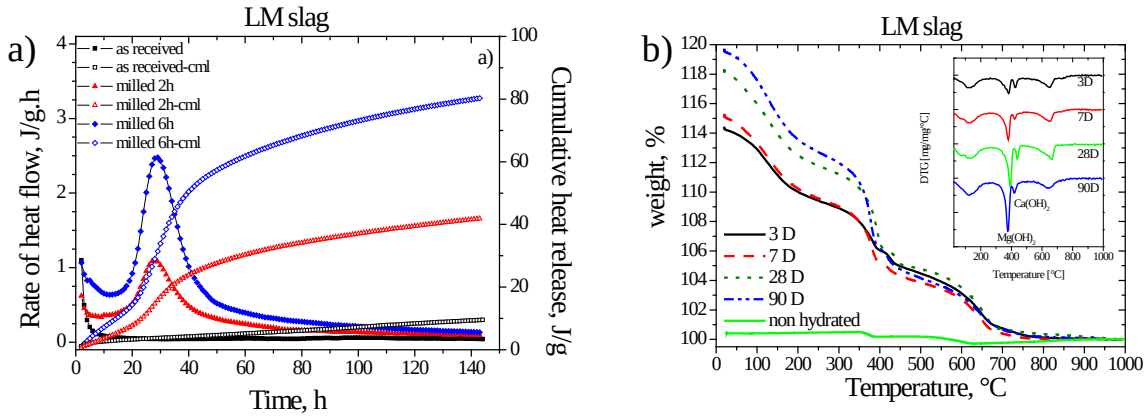

Figure 5. (a) Calorimetry results of mechanically activated slags; (b) TG and DTG curves (insert figure) of hydrated LM slag after 3, 7, 9, 28 and 90 days.

As the C-S-H phase has a poorly crystalline structure that does not give clear diffraction peaks in XRD patterns, the hydration process could be indirectly tracked by monitoring the growth of the amorphous fraction [25]. The latter increased significantly with hydration time, Table 4. After 28 days of hydration, the amorphous content was estimated at 64 wt.% and 71 wt.% for LM and AOD slag (data not shown), respectively. In terms of crystalline phases, the major phases originally present in slag decrease with hydration time and new phases, being the reaction products of the

occurring hydration, are detected (Table 4). In particular, high reaction rates are recorded for β- and γ-C_2S, merwinite and periclase, especially for the first 3 days of hydration. Bredigite is also decreasing but at a slower rate. Regarding cuspidine, in LM slag, it decreases during the first 3 days then it remains stable; in AOD slag (data not shown) it is present in very low concentration which remains practically constant. New phases, CH, being the reaction product most probably of C_2S, and calcite, formed after the carbonation of CH, were detected. In addition, brucite gradually appears in the system resulting from the hydration of periclase. The quantity of brucite determined by QXRD is relatively low, despite the high initial content of periclase, and its content diminishes as hydration advances, which is an indication that it hydrates. The dilution effect in view of the increasingly bounded crystalline water can not suffice alone as an interpretation. Most probably the reaction product from periclase is poorly crystalline and/or the Rietveld quantification underestimates its content. As a result, in both events described above, a fraction from the hydration of periclase is calculated as amorphous phase in Table 4. Thus, the amorphous phase alone should not be treated as a quantitative indication of C-S-H growth.

Table 4. Evolution of phases during hydration for LM slag based on Rietveld analysis, in wt.%.

Phase	Milled 6h	3 days	7 days	28 days	90 days
γ – dicalcium silicate	24	17	16	13	13
β – dicalcium silicate	4	< 1	< 1	n/a	n/a
Merwinite	5	4	3	3	2
Bredigite	6	4	4	2	< 1
Periclase	12	6	4	1	< 1
Cuspidine	12	8	9	7	7
Portlandite	< 1	1	1	2	1
Brucite	n/a	1	2	3	3
Others/Amorphous	29	51	53	64	67

The TGA/DTG curves, Fig. 5(b), show a number of characteristics peaks and an overall weight loss that increases as hydration times advances. The weight loss of both non hydrated slag samples is negligible compared to the hydrated ones, Fig. 5 (b). In more detail, for LM slag the weight loss is 12.6%, 13.2%, 15.5% and 16.4% for 3, 7, 28 and 90 days of hydration respectively. Recalculation by dividing with the hydrating days (assuming linear weight gain over the designated periods) shows that the hydration rate, expressed in weight gain per day, is significantly higher the first 3 days. As hydration advances, hydration rates are gradually diminishing. A comparable trend is observed for AOD slag; weight loss is lower in this case, e.g. for 3 days is 11.2% and reaches 15.5% in 90 days. These findings are in agreement with XRD analysis, where high reaction rates were also observed for the first 3 days.

In terms of specific reactions based on TGA, calculations were performed in accordance to the method proposed by Taylor [21], described in formula (1) for the dehydration of CH (changed accordingly for MH):

$$\mathrm{Ca(OH)_2}[\%] = WL_{\mathrm{Ca(OH)_2}}[\%] \times \frac{MW_{\mathrm{Ca(OH)_2}}}{MW_{H_2O}} \quad (1)$$

where $WL_{\mathrm{Ca(OH)_2}}$ is the weight loss during the dehydration of CH and $MW_{\mathrm{Ca(OH)_2}}$ and $MW_{\mathrm{H_2O}}$ are the molecular

weights of CH and water respectively.

In the case of LM slag, 1.8 wt.% of CH was determined after 3 days of hydration. This CH content stayed practically stable during the entire studied hydration period. Rietveld analysis gave comparable values, ranging from 1.4 wt.% for 3 days of hydration to 1.0 wt.% for 90 days of hydration. For AOD slag there is no peak in the TGA curve, in the temperature range 425 °C – 550 °C, which could be associated with CH presence. This finding is in reasonable agreement with results from Rietveld analysis (Table 4), indicating CH content below 1 wt.%. The above findings are in accord with other works [25] as well, where comparable values between Rietveld analysis and TGA were found for CH. For brucite (MH), results indicate high formation rates for both slags in the first 3 days of hydration and gradually diminishing rates as hydration progresses. In 90 days, approximately 10 wt.% and 9 wt.% of MH has been formed in LM and AOD slag respectively. As already commented, data from Rietveld analysis are not reflecting the expected MH formation and the present TG findings also verify the above.

The hydration process of LM slag is monitored for the first 90 days by SEM, Fig. 6 (a), (b). It is evident that gel-like structures resembling C-S-H phase have formed. LM slag hydrates with flake-like morphology at early stage growing to form a reticulated network at a later stage of hydration. In the case of AOD slag, the hydration starts with the formation of needles radiating from grains, forming spherical dense agglomerates as the hydration continuous. In both slags, the reticular network is visible even after 90 days of hydration. A substantial amount of porosity is present, especially in case of AOD sample (data not shown).

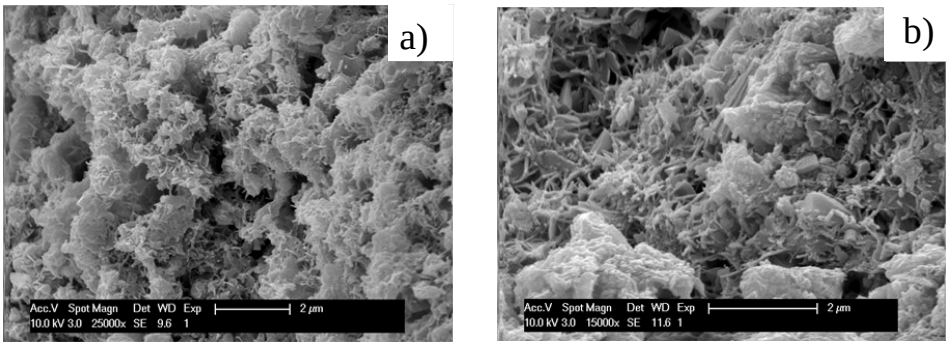

Figure 6. SE micrographs of LM slag a) 3D, b) 90D.

5. Proposed reaction scheme

The reaction scheme proposed focuses on the behavior of main phases present, i.e. γ-C_2S, merwinite, bredigite and periclase. Results demonstrate that all these phases decrease significantly, especially during the first three days of hydration (Table 4).

Gamma-C_2S, when activated, hydrates similarly to β-C_2S and forms C-S-H gel and CH [11]. Produced CH could act as a chemical activator in the next steps of hydration. As there was more γ-C_2S in LM slag compared to AOD slag, more CH was produced during hydration. The additional chemical activation caused by CH could be a reason for the higher reaction rate of γ-C_2S in LM slag compared to AOD. In both slags, the amount of CH does not increase with hydration time as it was expected. This phenomenon could be explained by the presence of MgO, which can hinder the

precipitation of CH [26, 27]. Results (Figure 5(b)) show that CH is mostly formed during the first three days of hydration and that the level stays relatively stable during the entire studied hydration period; on the contrary, the content of brucite increased gradually during the entire hydration period.

Regarding merwinite and bredigite, their hydration cannot be explicitly proven although their relative amounts decreased during hydration. Regarding merwinite, Muhmood *et al*. [28] observed that reducing the grain size enhances its dissolution kinetics in water and makes it highly hydraulic whereas Qian *et al.* reported that it hydrates under hydrothermal condition to form a Mg^{2+} containing C-S-H structure (Mg-calcio-chondrodite, tobermorite, Mg-gyrolite, Mg-truscottile and Mg-xonotlite) that strongly depends on the temperature and (C+M)/S ratio [29]. Similarly, the hydration of bredigite in an alkaline environment has been suggested before [23]. Still, no exact hydration reaction scheme has been described in the literature for merwinite and bredigite to the best of our knowledge.

Periclase reacts with water producing brucite. Generally, this reaction is slow and accompanied by volume increase causing "late swelling" effect [30]. In the present case, due to the fine particle size, the hydration kinetics are considerably fast and it is doubtful if periclase presence is indeed problematic.

6. Conclusions

The present work demonstrated that metastable slags show hydraulic properties. This was achieved either by rapid quenching, where the high-temperature polymorph of β-C_2S was stabilised and became the main hydraulic phase, or by prolonged milling, where the reactivity of γ-C_2S was enhanced. In more detail:

- Solidification of highly basic synthetic slags by means of melt spinning granulation or water quenching can prevent the β to γ transformation. The cooling technique has a notable impact on the mineralogical composition of final material.
- Beta and γ-C_2S, merwinite and bredigite are the major phases in the solidified slags. As the basicity increases, C_2S becomes the main phase.
- The granulated slags show hydraulic activity which is more pronounced for higher basicity due to the higher β-C_2S content.
- Mechanical activation of industrial (slowly cooled) slags via prolonged milling caused an increase in the XRD amorphous phase and a decrease in γ-C_2S, merwinite, bredigite, periclase and fluorite.
- The mechanical activation significantly increased the hydraulic reactivity of the slag. The amount of heat released per surface area increased with milling time, indicating that the surface is not the only factor influencing reactivity.
- During hydration, the amount of C_2S, merwinite, bredigite and periclase decreased whereas brucite and the amorphous phase increased, indicating the hydraulic nature of the material.
- The main hydration products according to TGA/DTG and SEM are most probably C-S-H gel, CH and MH.

Acknowledgements

The authors gratefully acknowledge Aperam and IWT O&O project 090594 for financial support. YP is thankful to the Research Foundation – Flanders for the post-doctoral fellowship.

References

[1] Ecofys, Methodology for the free allocation of emission allowances in the EU ETS post 2012, in, Sector report for the cement industry, by order of the European Commission, 2009.

[2] http://www.iea.org/papers/2009/Cement_Roadmap_targets_viewing.pdf, (16.12.2011).

[3] Worrell, E., Price, L., Martin, N., Hendriks, C., Meida, L.O., Carbon dioxide emissions from the global cement industry, Annual Review of Energy and the Environment, 26 (2001) 303-329.

[4] Cement Technology Roadmap 2009, Carbon emmision reductions up to 2050, World Business Council for Sustainable Development.

[5] Shen, H., Forssberg, E., Nordström, U., Physicochemical and mineralogical properties of stainless steel slags oriented to metal recovery, Resour. Conserv. Recy., 40 (2004) 245-271.

[6] Wang, R., Chen, R., Beneficial use of stainless steel AOD slag as composite cement admixture and its safety analysis, in: Waste Recovery in Ironmaking and Steelmaking Processes, The Institute of Materials, Minerals and Mining, London, 2010.

[7] Faraone, N., Tonello, G., Furlani, E., Maschio, S., Steelmaking slag as aggregate for mortars: Effects of particle dimension on compression strength, Chemosphere, 77 (2009) 1152-1156.

[8] Setién, J., Hernández, D., González, J.J., Characterization of ladle furnace basic slag for use as a construction material, Constr. Build. Mater., 23 (2009) 1788-1794.

[9] Rodriguez, Á., Manso, J.M., Aragón, Á., Gonzalez, J.J., Strength and workability of masonry mortars manufactured with ladle furnace slag, Resour. Conserv. Recy., 53 (2009) 645-651.

[10] Shi, C., Characteristics and cementitious properties of ladle slag fines from steel production, Cem. Concr. Res., 32 (2002) 459-462.

[11] Shi, C., Hu, S., Cementitious properties of ladle slag fines under autoclave curing conditions, Cem. Concr. Res., 33 (2003) 1851-1856.

[12] Yang, Q., Engström, F., Björkman, B., Adolfsson, D., Modification study of a steel slag to prevent the slag disintegration after metal recovery and to enhance slag utilization, in: Mario Sánchez, Roberto Parra, Gabriel Riveros, Carlos Díaz (Eds.) 8th International Conference on Molten Slags, Fluxes and Salts – MOLTEN 2009, Santiago, Chile, 2009.

[13] Kumar, S., Bandopadhyay, A., Rajinikanth, V., Alex, T.C., Kumar, R., Improved processing of blended slag cement through mechanical activation, J. Mater. Sci., 39 (2004) 3449-3452.

[14] Kumar, S., Kumar, R., Bandopadhyay, A., Innovative methodologies for the utilisation of wastes from metallurgical and allied industries, Resour. Conserv. Recy., 48 (2006) 301-314.

[15] Bouzoubaâ, N., Zhang, M.H., Bilodeau, A., Malhotra, V.M., The effect of grinding on the physical properties of fly ashes and a portland cement clinker, Cem. Concr. Res., 27 (1997) 1861-1874.

[16] Knapen, E., Cizer, Ö., Van Balen, K., Van Gemert, D., Effect of free water removal from early-age hydrated cement pastes on thermal analysis, Constr. Build. Mater., 23 (2009) 3431-3438.

[17] Juckes, L.M., Dicalcium silicate in blast-furnace slag: A critical review of the implications for aggregate stability, Transactions of the Institution of Mining and Metallurgy, Section C: Mineral Processing and Extractive Metallurgy, 111 (2002).

[18] Groves, G.W., Phase transformations in dicalcium silicate, J. Mater. Sci., 18 (1983) 1615-1624.

[19] Alanyali, H., Çöl, M., Yilmaz, M., Karagöz, Ş., Concrete Produced by Steel-Making Slag (Basic Oxygen Furnace) Addition in Portland Cement, International Journal of Applied Ceramic Technology, 6 (2009) 736-748.

[20] Ramachandran, V.S., Paroli, R.M., Beaudoin, J.J., Delgado, A.H., Handbook of Thermal Analysis of Constructions Materials, Noyes Publications, Norwich, U.S.A, (2002).

[21] Taylor, H.F.W., Cement Chemistry, 2nd ed., 1997.

[22] McCarthy, G.J., Grier, D.G., Wisdom, M.A., Peterson, R.B., Lerach, S.L., Jarabek, R.L., Walsh, J.J., Winburn, R.S., Coal Combustion By-Product Diadenesis II, Internation Ash Utilization Symposium, Kentucky, USA, (1999).

[23] Moseley, D., Glasser, F.P., Properties and composition of bredigite-structured phases J. Mater. Sci., 17 (1982) 2736-2740.

[24] Venkateswaran, D., Sharma, D., Muhmood, L., Vitta, S., Treatment and characterisation of electric arc furnace (EAF) slag for its effective utilisation in cementitious products, Global slag magazine, October (2007).

[25] Scrivener, K.L., Füllmann, T., Gallucci, E., Walenta, G., Bermejo, E., Quantitative study of Portland cement hydration by X-ray diffraction/Rietveld analysis and independent methods, Cem. Concr. Res., 34 (2004) 1541-1547.

[26] Fernandez, L., Alonso, C., Hidalgo, A., Andrade, C., The role of magnesium during the hydration of C_3S and C-S-H formation. Scanning electron microscopy and mid-infrared studies, Adv. Cem. Res., 17 (2005) 9-21.

[27] Zheng, L., Xuehua, C., Mingshu, T., Hydration and setting time of MgO-type expansive cement, Cem. Concr. Res., 22 (1992) 1-5.

[28] Muhmood, L., Vitta, S., Venkateswaran, D., Cementitious and pozzolanic behavior of electric arc furnace steel slags, Cem. Concr. Res., 39 (2009) 102-109.

[29] Qian, G., Li, A., Xu, G., Li, H., Hydrothermal products of the C3MS2-C12A7-MgO system, Cem. Concr. Res., 27 (1997) 1791-1797.

[30] Lea's Chemistry of Cement and Concrete, Hewlett, P. C. (Ed), (2004).